Geophysical Research Letters

RESEARCH LETTER
10.1029/2022GL099116

Key Points:

- Iron is strongly incompatible in the (Mg,Fe)O system
- Crystals in equilibrium with liquid are buoyant in this system at high pressure
- The iron spin transition causes the distribution coefficient to depend non-monotonically on pressure

Correspondence to:

L. Stixrude,
lstixrude@epss.ucla.edu

Citation:

Braithwaite, J., & Stixrude, L. (2022). Partitioning of iron between liquid and crystalline phases of (Mg,Fe)O. *Geophysical Research Letters*, *49*, e2022GL099116. https://doi.org/10.1029/2022GL099116

Received 12 APR 2022
Accepted 17 AUG 2022

Author Contributions:

Conceptualization: Lars Stixrude
Formal analysis: James Braithwaite, Lars Stixrude
Funding acquisition: Lars Stixrude
Investigation: Lars Stixrude
Methodology: James Braithwaite, Lars Stixrude
Project Administration: Lars Stixrude
Software: James Braithwaite, Lars Stixrude
Supervision: Lars Stixrude
Validation: James Braithwaite, Lars Stixrude
Writing – review & editing: Lars Stixrude

Partitioning of Iron Between Liquid and Crystalline Phases of (Mg,Fe)O

James Braithwaite[1] **and Lars Stixrude**[1,2]

[1]Department of Earth Sciences, University College London, London, UK, [2]Now at Department of Earth, Planetary, and Space Sciences, University of California, Los Angeles, CA, USA

Abstract The density contrast between crystals and coexisting liquids is key to understanding the evolution of the magma ocean. While crystals remain denser than isochemical liquids in most oxide and silicate systems over the pressure range of Earth's mantle, element partitioning, particularly of abundant heavy elements such as iron, can alter the buoyancy. We use molecular dynamics simulations based on spin-polarized density functional theory and adiabatic switching to determine the free energy of iron substitution in liquid and crystalline (Mg,Fe)O and the distribution coefficient. We find that iron is strongly incompatible with a distribution coefficient less than 0.3 over the mantle pressure range. We find that the crystal is buoyant with respect to coexisting liquid at pressures exceeding 50 GPa. The high-spin to low-spin transition has an important influence on the distribution coefficient, which decreases with increasing pressure up to 80 GPa, and then increases on further increase of pressure.

Plain Language Summary Near Earth's surface, where most magma is generated today, crystals usually sink in magma because they are denser than liquid. But we find that at high pressure liquid is much more rich in iron than crystals, which means that crystals can float in the deep Earth. This behavior is important for understanding the earliest stages of Earth's evolution when it may have been completely molten.

1. Introduction

The early Earth may have been extensively or completely molten, and it has been proposed that as the silicate portion crystallized, a basal magma ocean formed: a layer of silicate liquid at the base of the mantle overlain by crystalline material (Labrosse et al., 2007). The formation of the basal magma ocean has been invoked to explain geochemical signatures from the mantle, the properties of deep mantle structures as revealed by seismology, including large low shear wave velocity provinces (LLSVPs), and ultra low velocity zones (ULVZs), and may have been the source of the Earth's earliest magnetic field (Stixrude et al., 2020).

The formation of a basal magma ocean requires silicate liquids to become denser than coexisting solids at high pressure. It is known that at low pressure, silicate liquids are less dense than coexisting crystalline assemblages, accounting for the rise of magma toward the surface (Lange & Carmichael, 1987). We also know that at lower mantle pressure, silicate liquids approach, but do not exceed the density of isochemical crystalline assemblages (Braithwaite & Stixrude, 2019; Stixrude & Karki, 2005). For silicate liquids to be denser than crystals requires the partitioning of elements: a difference in composition between coexisting phases dictated by chemical equilibrium that leaves the liquid enriched in relatively abundant and massive elements such as iron (Stixrude et al., 2009).

The nature of element partitioning between silicate liquid and coexisting crystals at lower mantle pressure is still poorly constrained. For example, experimentally determined values of the distribution coefficient of iron between silicate liquid and bridgmanite range from 0.09 to 0.5 (Andrault et al., 2012; Nomura et al., 2011). In the (Mg,Fe)O system experimentally determined values of the distribution coefficient also span a wide range (Deng & Lee, 2017; Du & Lee, 2014; Fu et al., 2018). To our knowledge, there have been no ab initio predictions of iron partitioning between liquid and crystalline phases in mantle oxide or silicate systems. The current state of knowledge therefore does not permit us to draw conclusions about the relative density of liquids and crystals in the lower mantle, nor the possible formation of a basal magma ocean.

Here, we investigate partitioning of iron between liquid and crystalline phases of (Mg,Fe)O. Depending on pressure, ferropericlase is found to be the second or third phase to crystallize from the magma ocean in the deep mantle (Fiquet et al., 2010; Tateno et al., 2014), and so iron partitioning in this system is important for under-

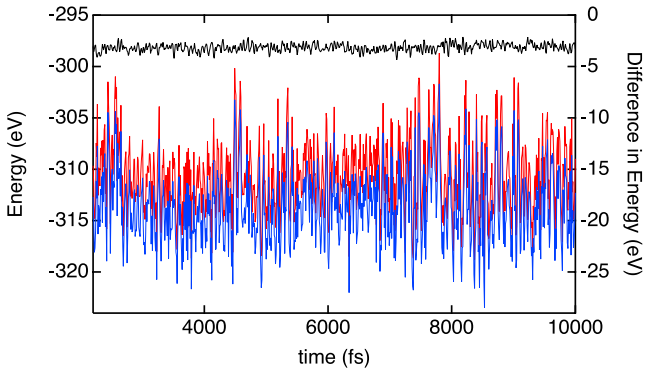

Figure 1. The internal energy of the liquid phase along an iron-free trajectory ($\lambda = 0$) for iron-free (U_0, red) and high-spin iron-bearing (U_1, blue) systems and the difference $\Delta U = U_1 - U_0$ (black, right axis) at 480 Å^3 per cell (4.518 cm^3 mol^{-1} atom^{-1}, 92 GPa), and 4000 K.

standing the formation and chemical evolution of a putative basal magma ocean. Moreover, (Mg,Fe)O is a relatively simple model system that allows us to isolate the influence of pressure on iron partitioning, and in particular, the role of the high spin to low spin transition of the ferrous cation.

2. Methods

We determine the partitioning of iron between liquid and crystalline phases of (Mg,Fe)O from first principles via adiabatic switching, a form of thermodynamic integration that has been widely used to study element partitioning (Alfe et al., 2002; Deng & Stixrude, 2021; Frenkel & Smit, 1996). In brief, the method computes the work done on the system by transmuting one or more Mg atoms to Fe atoms, and relates this to the free energy of cation exchange, from which the distribution coefficient is calculated.

In the dilute limit which is our focus, the distribution coefficient

$$K_D \equiv \frac{x_C\,(1-x_L)}{x_L\,(1-x_C)} = \exp\left(-\frac{\Delta G_R}{kT}\right) \tag{1}$$

where $x_A = \mathrm{Fe}/(\mathrm{Fe}+\mathrm{Mg})$, $A = L$ (liquid) or $A = C$ (crystal) denotes the phase, ΔG_R is the free energy change of the reaction

$$\mathrm{MgO}\ \ (\mathrm{crystal}) + \mathrm{FeO}\ \ (\mathrm{liquid}) = \mathrm{MgO}\ \ (\mathrm{liquid}) + \mathrm{FeO}\ \ (\mathrm{crystal}) \tag{2}$$

for which the free energy of reaction may be divided into single phase components

$$\Delta G_R = \Delta G_C - \Delta G_L \tag{3}$$

with

$$\Delta G_A = G_A(\mathrm{FeO}) - G_A(\mathrm{MgO}) \tag{4}$$

We find the Helmholtz free energy of chemical substitution via adiabatic switching

$$\Delta F = \int_0^1 \langle \Delta U \rangle_\lambda \, d\lambda \tag{5}$$

where λ specifies the Hamiltonian that produces the molecular dynamics trajectory: $\lambda = 1$ for the iron-bearing trajectory and $\lambda = 0$ for the iron-free trajectory, $U = E - TS_{\mathrm{el}} - TS_{\mathrm{mag}}$, where E is the internal energy, T is temperature, S_{el} is the electronic entropy, S_{mag} is the magnetic entropy, and $\langle \Delta U \rangle$ is the time averaged difference between U_1 and U_0: the values of U for the iron-bearing and iron-free systems, respectively. We take $S_{\mathrm{mag}} = k\ln(\mu + 1)$ per iron atom with μ the local magnetic moment on the iron atom in units of Bohr magnetons. Because fluctuations in ΔU are small compared with $\langle \Delta U \rangle$ and kT, we compute the integral as (Sola & Alfe, 2009)

$$\Delta F = \frac{1}{2}\left(\langle \Delta U \rangle_1 + \langle \Delta U \rangle_0\right) \tag{6}$$

A typical trajectory of ΔU is shown in Figure 1.

Finally, we relate the Gibbs free energy to the Helmholtz free energy of substitution (Desjarlais, 2013)

$$\Delta G_R\,(P_D) = \Delta F_C\,(V, T\ :\ P_C) - \Delta F_L\,(V, T\ :\ P_L) \tag{7}$$

with

$$P_D = \frac{P_L\sqrt{k_L} + P_C\sqrt{k_C}}{\sqrt{k_L} + \sqrt{k_C}} \tag{8}$$

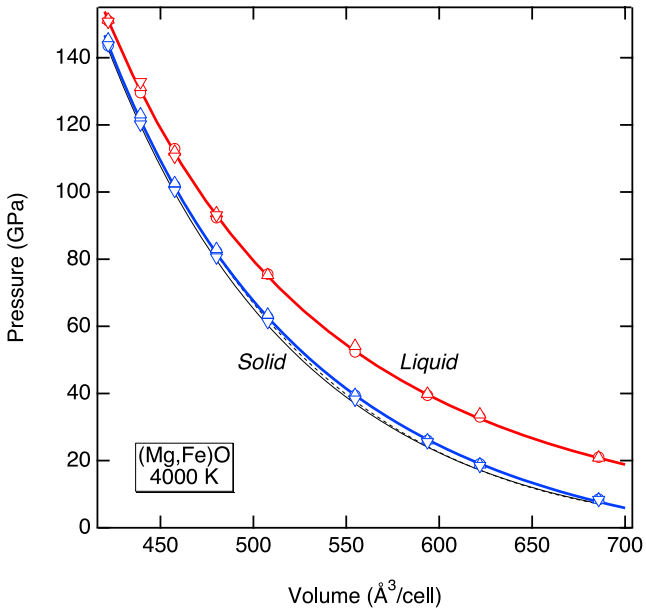

Figure 2. Equation of state of crystalline (blue) and liquid (red) phases in Fe-free (circles) and Fe-bearing (high-spin: up triangle, low-spin: down triangle) compositions with $x_A = 1/32$ (3.125%). The symbols are the results of our simulations and the lines are third-order Birch-Murnaghan equation of state fits to the simulation results. Also shown for comparison is the experimental 4000 K isotherm (black lines; solid: Birch-Murnaghan, dashed: Vinet) (Tange et al., 2009).

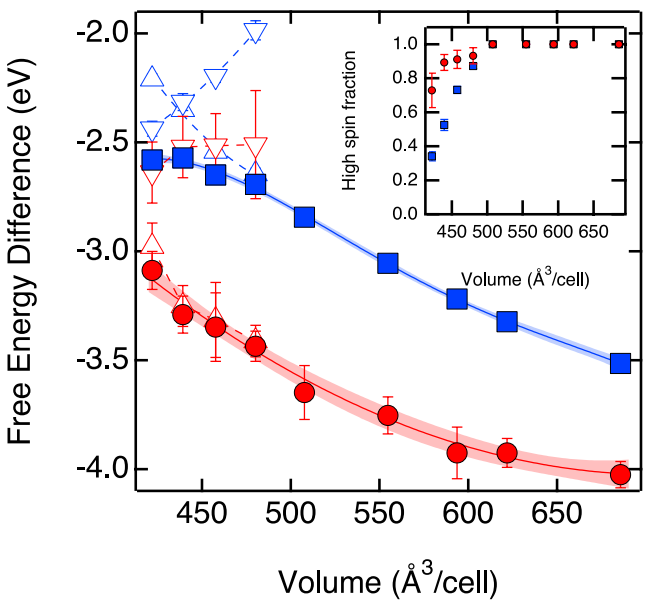

Figure 3. The free energy change upon iron substitution ΔF in crystalline (solid blue squares) and liquid (solid red circles) phases. The solid lines are polynomial fits to the results with the uncertainty in the fit indicated by the shading. We also show results for fixed high-spin (upward pointing triangles) and low-spin (downward pointing triangles) for crystalline (blue) and liquid (red) phases. The inset shows the equilibrium value of the high-spin fraction in crystalline (blue squares) and liquid (red circles) phases.

where P_A are the pressures computed from Fe-free trajectories of each phase and k_A are the isothermal compressibilities (inverse of the bulk modulus) computed from Birch-Murnaghan fits to the equations of state of the crystalline ($A = C$) and liquid ($A = L$) phases. The equations of state are shown in Figure 2.

The details of our first principles molecular dynamics simulations follow our previous work on liquid and crystalline phases of (Mg,Fe)O (Holmstrom & Stixrude, 2015, 2016). Briefly, the simulations are based on density functional theory in the PBEsol approximation (Perdew et al., 2008) combined with the + U method (Dudarev et al., 1998) with $U - J = 2.5$ eV. We use the projector augmented plane wave method as implemented in VASP (Kresse & Furthmuller, 1996; Kresse & Joubert, 1999). The outermost core radii (in Bohr) and number of electrons treated as valence are: Fe (2.2, 14), Mg (2, 8), and O (1.52, 6). We perform Born-Oppenheimer simulations in the canonical ensemble with the Nosé-Hoover thermostat for typically 10 ps with 1 fs time step. We assume thermal equilibrium between ions and electrons via the Mermin functional (Mermin, 1965). Sampling the Brillouin zone at the Gamma point and a basis-set energy cutoff of 500 eV was found to be sufficient to converge ΔU and pressure to within 0.07 eV and 0.2 GPa, respectively.

We consider simulation cells of 64 atoms with periodic boundary conditions in liquid and crystalline phases of pure MgO composition and with one Fe substitution, corresponding to $x_A = 1/32 = 3.125\%$. We perform spin-polarized calculations with the spin moment on the iron atom either free to vary, or fixed to the high-spin ($\mu = 4$) or low-spin ($\mu = 0$) states. We find the stable magnetic state is high spin up to 80 GPa. At higher pressure, we determine the equilibrium value of μ by minimizing ΔF with respect to the high spin fraction

$$\Delta F = (1 - f)\Delta F_{LS} + f\Delta F_{HS} + kT\,[f \ln f + (1 - f)\ln(1 - f)] \quad (9)$$

where the equilibrium high spin fraction

$$f = \left\{1 + \exp\left[\left(\Delta F_{HS} - \Delta F_{LS}\right)/kT\right]\right\}^{-1} \quad (10)$$

and ΔF_{LS} and ΔF_{HS} are the values computed for fixed high-spin and low-spin states, respectively.

3. Results

The free energy of iron substitution in the liquid is less than that in the solid over the entire range of volume explored here (Figure 3). This means that Fe partitions preferentially into the liquid phase (i.e., Fe is incompatible). The variation of ΔF on compression is influenced by the high-spin to low-spin transition in both phases, but much more so in the crystal. The high-spin to low-spin transition occurs over a broad range of pressure in both phases (Figure 3 inset). The gradual transition begins at volume <508 Å^3/cell (for which the pressure is 68 and 80 GPa in crystal and liquid, respectively). The crystal is mostly low-spin ($f = 0.35$) at the smallest volume explored in our study (422 Å^3/cell, corresponding to 145 GPa), whereas the liquid remains mostly high-spin over the entire range explored ($f > 0.7$).

The distribution coefficient is much less than unity over the entire range explored indicating strong partitioning of Fe into the liquid phase (Figure 4).

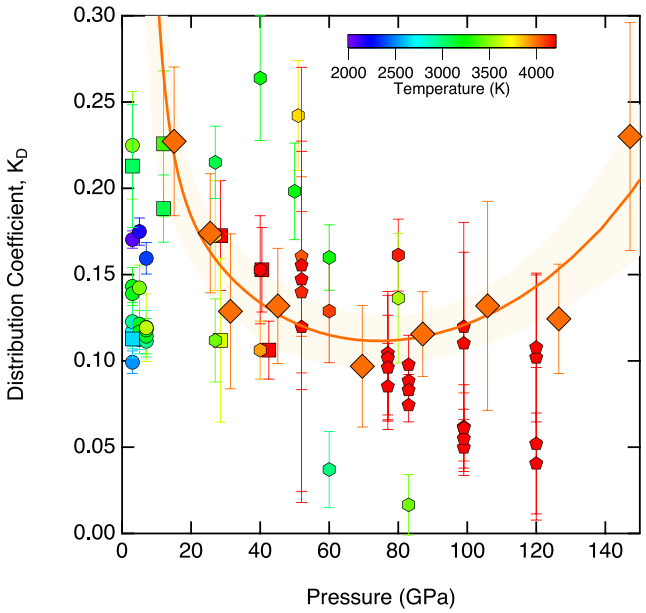

Figure 4. The distribution coefficient from our results (large orange diamonds and orange line with orange shading) compared with experimental results: circles (Zhang & Fei, 2008); squares (Du & Lee, 2014); hexagons (Deng & Lee, 2017); pentagons (Fu et al., 2018). All theoretical and experimental results are color coded according to the temperature. The theoretical line and its uncertainty are computed from the polynomial fits to ΔF of solid and liquid phases (Figure 3).

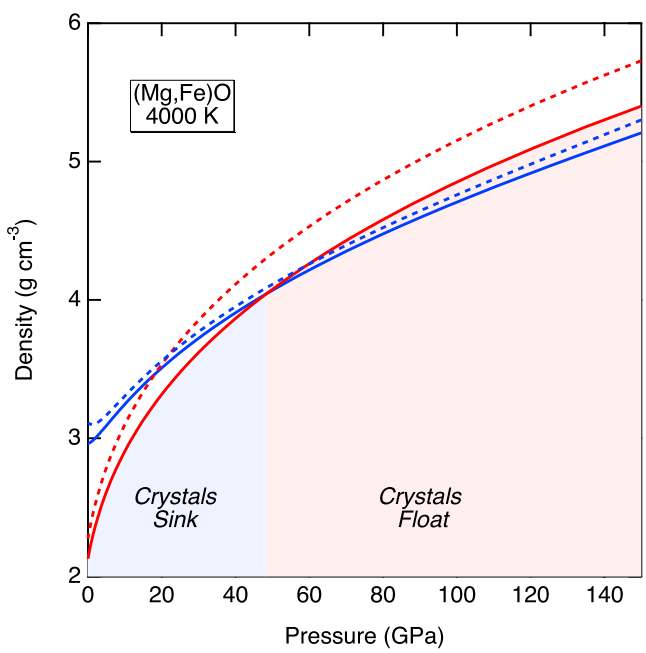

Figure 5. The density of liquid (red) and coexisting crystal (blue) for $x_L = 0.1$ (solid lines) and $x_L = 0.2$ (dashed lines). The shading indicates the range of pressure over which the liquid is less dense (crystals sink) and more dense (crystals float) than the coexisting crystalline phase.

The distribution coefficient decreases with increasing pressure at low pressure, reaches a minimum near 80 GPa, and then increases with increasing pressure at higher pressure. The change in pressure dependence of K_D is caused by the high-spin to low-spin transition in the crystal.

Our results agree with trends that are apparent in experimental data: experiments also show small values of the distribution coefficient ($K_D < 0.3$), and a tendency for the value of K_D to decrease with increasing pressure at least up to a pressure of 70 GPa. A more detailed comparison is limited by the fact that most experiments are performed at different temperatures than ours and on more iron rich compositions. The dependence of the distribution coefficient on iron content is not clear, but some studies report that they are able to account for their results with the ideal solution approximation, for which the distribution coefficient is independent of iron concentration (Fu et al., 2018; Zhang & Fei, 2008), suggesting that it is reasonable to compare our results with experimental data despite differences in iron concentration. The dependence of K_D on iron concentration may become important for the most iron-rich compositions, such as the lowest temperature results of (Zhang & Fei, 2008), for which $x_L > 0.9$.

The density of (Mg,Fe)O liquid exceeds that of coexisting (Mg,Fe)O crystal over most of the mantle pressure regime (Figure 5). The composition of the crystal in equilibrium with a liquid of composition x_L is, from the definition of K_D

$$x_C = \left(\frac{1 - x_L}{K_D x_L} + 1 \right)^{-1} \tag{11}$$

which yields, for example, $x_C = 0.016$ for $K_D = 0.15$, and $x_L = 0.1$. We consider values of $x_L = 0.1$, representative of the bulk silicate Earth, and a putative global magma ocean, and $x_L = 0.2$, representative of a global magma ocean that is iron-enriched (e.g., due to crystallization). We compute the iron concentration of the coexisting crystalline phase using Equation 11 and our distribution coefficient (Figure 4). The density of phase A is

$$\rho_A = \frac{w^{\mathrm{FeO}} x_A + w^{\mathrm{MgO}} (1 - x_A)}{V_A^{\mathrm{FeO}} x_A + V_A^{\mathrm{MgO}} (1 - x_A)} \tag{12}$$

where w^i and V_A^i are, respectively, the molecular masses and volumes of the end-members. We use our iron free results for V_A^{MgO} (Figure 2). For V_A^{FeO} we focus on the high-spin state since the density crossover occurs at a pressure much lower than that of the spin transition for either phase. We assume $V_A^{\mathrm{FeO}} - V_A^{\mathrm{MgO}} = 0.9$ cm^3 mol^{-1}, for both phases, consistent with our present and previous results (Munoz-Ramo & Stixrude, 2014).

4. Discussion

Our finding that the liquid phase is denser than the crystalline phase in the (Mg,Fe)O system is significant for our understanding of crystal buoyancy in the magma ocean. The magma ocean differs in composition from the system that we have studied here, most notably in the addition of the silica component. We have found that at constant pressure and temperature, the density of silicate liquids increases with increasing silica content at lower mantle pressures (de Koker et al., 2013). Therefore, ferropericlase crystals are even more buoyant in the magma ocean than they are in the (Mg,Fe)O system. Buoyant rise of ferropericlase in a crystallizing magma ocean is important because it

leaves behind liquid that becomes increasingly rich in iron and other incompatible elements. The enrichment of a basal magma ocean has previously been invoked as a possible explanation for the origin of LLSVP, ULVZ, and various geochemical signatures as seen in plume-derived lavas (Labrosse et al., 2007).

The pressure of the high spin to low spin transition that we find is consistent with that found in previous ab initio studies. For example, in the solid phase, we find $f = 0.5$ at 121 GPa, as compared with 130 GPa for $x_C = 0.25$ (Holmstrom & Stixrude, 2015). The increase of transition pressure with increasing x_C has been found in a number of experimental and theoretical studies, albeit mostly at low temperature (Persson et al., 2006; Solomatova et al., 2016). Our results are consistent with a previous theoretical study on ferropericlase showing that the trend toward increasing stabilization of the high spin state with increasing x_C persists at high temperature (Muir & Brodholt, 2015). In the liquid phase, we find that the spin transition occurs at higher pressure than in the solid phase, consistent with our previous study of the liquid phase at $x_L = 0.25$ (Holmstrom & Stixrude, 2016).

Comparison with a previous, approximate ab initio study provides additional insight into our results. The previous study (Ghosh & Karki, 2016) finds a much larger value of K_D than we do and that K_D increases monotonically with increasing pressure with K_D varying from 0.3 to 0.57 from 23 to 135 GPa at 4000 K. In contrast, we find smaller values of K_D at all pressures and a non-monotonic variation with pressure. These different results are due to two approximations in the previous study: (a) that iron is in the low spin state at all pressures (non-spin-polarized) and (b) that the Gibbs free energy of reaction (Equation 3) is equal to the enthalpy of reaction, thus neglecting the entropy of reaction. We find that as iron goes through the high-spin to low-spin transition, it becomes more compatible, with the value of K_D increasing as the spin transition proceeds. The much smaller value of K_D that we find is important for understanding crystal buoyancy. With K_D as large as 0.57, as in the previous study, crystals are much less buoyant than we find: the liquid with $x_L = 0.1$ is less dense than the coexisting crystal up to a pressure of 115 GPa.

5. Conclusion

Iron behaves as a very incompatible element in the (Mg,Fe)O system: it partitions strongly into the liquid. Because of strong iron partitioning, ferropericlase crystals are buoyant with respect to coexisting liquid and are likely to rise in a crystallizing deep magma ocean. We have shown that it is possible to compute ab initio the partitioning of iron between liquid and crystalline phases taking account of all relevant aspects of the physics, including strong correlation and spin polarization. The latter is important as the high-spin to low-spin transition of the ferrous iron cation has a major influence on the distribution coefficient, causing it to depend non-monotonically on pressure. The methods illustrated here are applicable to iron partitioning in other systems, including silicates, and to the partitioning of other elements between liquid and crystal silicates and oxides (Deng & Stixrude, 2021).

Data Availability Statement

Data are available in the Open Science Framework (https://osf.io/udfth/) with DOI: https://doi.org/10.17605/OSF.IO/UDFTH.

Acknowledgments
This project is supported by the National Science Foundation under grant EAR-1853388 to LS. Calculations were carried out using the IRIDIS cluster partly owned by University College London, ARCHER of the UK national high-performance computing service, and MARENOSTRUM at the Barcelona Supercomputing Center, Spain of the PRACE Consortium, and the Hoffman2 Shared Cluster provided by UCLA Institute for Digital Research and Education's Research Technology Group.

References

Alfe, D., Gillan, M. J., & Price, G. D. (2002). Ab initio chemical potentials of solid and liquid solutions and the chemistry of the Earth's core. *Journal of Chemical Physics*, *116*(16), 7127–7136. https://doi.org/10.1063/1.1464121

Andrault, D., Petitgirard, S., Nigro, G. L., Devidal, J. L., Veronesi, G., Garbarino, G., & Mezouar, M. (2012). Solid-liquid iron partitioning in Earth's deep mantle. *Nature*, *487*(7407), 354–357. https://doi.org/10.1038/nature11294

Braithwaite, J., & Stixrude, L. (2019). Melting of $CaSiO_3$ perovskite at high pressure. *Geophysical Research Letters*, *46*(4), 2037–2044. https://doi.org/10.1029/2018gl081805

de Koker, N., Karki, B. B., & Stixrude, L. (2013). Thermodynamics of the MgO-SiO_2 liquid system in Earth's lowermost mantle from first principles. *Earth and Planetary Science Letters*, *361*, 58–63. https://doi.org/10.1016/j.epsl.2012.11.026

Deng, J., & Lee, K. K. M. (2017). Viscosity jump in the lower mantle inferred from melting curves of ferropericlase. *Nature Communications*, *8*(1), 1997. https://doi.org/10.1038/s41467-017-02263-z

Deng, J., & Stixrude, L. (2021). Deep fractionation of Hf in a solidifying magma ocean and its implications for tungsten isotopic heterogeneities in the mantle. *Earth and Planetary Science Letters*, 562. https://doi.org/10.1016/j.epsl.2021.116873

Desjarlais, M. P. (2013). First-principles calculation of entropy for liquid metals. *Physical Review E*, *88*(6), 062145. https://doi.org/10.1103/physreve.88.062145

Du, Z. X., & Lee, K. K. M. (2014). High-pressure melting of MgO from (Mg, Fe)O solid solutions. *Geophysical Research Letters*, *41*(22), 8061–8066. https://doi.org/10.1002/2014gl061954

Dudarev, S. L., Botton, G. A., Savrasov, S. Y., Humphreys, C. J., & Sutton, A. P. (1998). Electron-energy-loss spectra and the structural stability of nickel oxide: An LSDA+U study. *Physical Review B*, *57*(3), 1505–1509. https://doi.org/10.1103/physrevb.57.1505

Fiquet, G., Auzende, A. L., Siebert, J., Corgne, A., Bureau, H., Ozawa, H., & Garbarino, G. (2010). Melting of peridotite to 140 gigapascals. *Science*, *329*(5998), 1516–1518. https://doi.org/10.1126/science.1192448

Frenkel, D., & Smit, B. (1996). *Understanding molecular simulation: From algorithms to applications*. Academic Press.

Fu, S. Y., Yang, J., Zhang, Y. J., Liu, J. C., Greenberg, E., Prakapenka, V. B., et al. (2018). Melting behavior of the lower-mantle ferropericlase across the spin crossover: Implication for the ultra-low velocity zones at the lowermost mantle. *Earth and Planetary Science Letters*, *503*, 1–9. https://doi.org/10.1016/j.epsl.2018.09.014

Ghosh, D. B., & Karki, B. B. (2016). Solid-liquid density and spin crossovers in (Mg, Fe)O system at deep mantle conditions. *Scientific Reports*, *6*(1), 37269. https://doi.org/10.1038/srep37269

Holmstrom, E., & Stixrude, L. (2015). Spin crossover in ferropericlase from first-principles molecular dynamics. *Physical Review Letters*, *114*(11), 117202. https://doi.org/10.1103/physrevlett.114.117202

Holmstrom, E., & Stixrude, L. (2016). Spin crossover in liquid (Mg, Fe)O at extreme conditions. *Physical Review B*, *93*(19), 195142. https://doi.org/10.1103/physrevb.93.195142

Kresse, G., & Furthmuller, J. (1996). Efficiency of ab-initio total energy calculations for metals and semiconductors using a plane-wave basis set. *Computational Materials Science*, *6*(1), 15–50. https://doi.org/10.1016/0927-0256(96)00008-0

Kresse, G., & Joubert, D. (1999). From ultrasoft pseudopotentials to the projector augmented-wave method. *Physical Review B*, *59*(3), 1758–1775. https://doi.org/10.1103/physrevb.59.1758

Labrosse, S., Hernlund, J. W., & Coltice, N. (2007). A crystallizing dense magma ocean at the base of the Earth's mantle. *Nature*, *450*(7171), 866–869. https://doi.org/10.1038/nature06355

Lange, R. A., & Carmichael, I. S. E. (1987). Densities of Na_2O-K_2O-CaO-MgO-FeO-Fe_2O_3-Al_2O_3-TiO_2-SiO_2 liquids - New measurements and derived partial molar properties. *Geochimica et Cosmochimica Acta*, *51*(11), 2931–2946. https://doi.org/10.1016/0016-7037(87)90368-1

Mermin, N. D. (1965). Thermal properties of the inhomogeneous electron gas. *Physical Review*, *137*(5A), A1441–A1443. https://doi.org/10.1103/physrev.137.a1441

Muir, J. M. R., & Brodholt, J. P. (2015). Elastic properties of ferropericlase at lower mantle conditions and its relevance to ULVZs. *Earth and Planetary Science Letters*, *417*, 40–48. https://doi.org/10.1016/j.epsl.2015.02.023

Munoz-Ramo, D., & Stixrude, L. (2014). Spin crossover in Fe_2SiO_4 liquid at high pressure. *Geophysical Research Letters*, *41*(13), 4512–4518. https://doi.org/10.1002/2014gl060473

Nomura, R., Ozawa, H., Tateno, S., Hirose, K., Hernlund, J., Muto, S., et al. (2011). Spin crossover and iron-rich silicate melt in the Earth's deep mantle. *Nature*, *473*(7346), 199–202. https://doi.org/10.1038/nature09940

Perdew, J. P., Ruzsinszky, A., Csonka, G. I., Vydrov, O. A., Scuseria, G. E., Constantin, L. A., et al. (2008). Restoring the density-gradient expansion for exchange in solids and surfaces. *Physical Review Letters*, *100*(13), 136406. https://doi.org/10.1103/physrevlett.100.136406

Persson, K., Ceder, G., Berta, A., & Morgan, D. (2006). Ab initio study of the composition dependence of the pressure-induced spin transition in the (Mg_1-xFex)O system. *Geophysical Research Letters*, *33*(16), L16306. https://doi.org/10.1029/2006gl026621

Sola, E., & Alfe, D. (2009). Melting of iron under Earth's core conditions from diffusion Monte Carlo free energy calculations. *Physical Review Letters*, *103*(7), 078501. https://doi.org/10.1103/physrevlett.103.078501

Solomatova, N. V., Jackson, J. M., Sturhahn, W., Wicks, J. K., Zhao, J. Y., Toellner, T. S., et al. (2016). Equation of state and spin crossover of (Mg, Fe)O at high pressure, with implications for explaining topographic relief at the core-mantle boundary. *American Mineralogist*, *101*(5–6), 1084–1093. https://doi.org/10.2138/am-2016-5510

Stixrude, L., de Koker, N., Sun, N., Mookherjee, M., & Karki, B. B. (2009). Thermodynamics of silicate liquids in the deep Earth. *Earth and Planetary Science Letters*, *278*(3–4), 226–232. https://doi.org/10.1016/j.epsl.2008.12.006

Stixrude, L., & Karki, B. (2005). Structure and freezing of $MgSiO_3$ liquid in Earth's lower mantle. *Science*, *310*(5746), 297–299. https://doi.org/10.1126/science.1116952

Stixrude, L., Scipioni, R., & Desjarlais, M. P. (2020). A silicate dynamo in the early Earth. *Nature Communications*, *11*(1), 935–940. https://doi.org/10.1038/s41467-020-14773-4

Tange, Y., Nishihara, Y., & Tsuchiya, T. (2009). Unified analyses for P-V-T equation of state of MgO: A solution for pressure-scale problems in high P-T experiments. *Journal of Geophysical Research: Solid Earth*, *114*(B3), B03208. https://doi.org/10.1029/2008jb005813

Tateno, S., Hirose, K., & Ohishi, Y. (2014). Melting experiments on peridotite to lowermost mantle conditions. *Journal of Geophysical Research: Solid Earth*, *119*(6), 4684–4694. https://doi.org/10.1002/2013jb010616

Zhang, L., & Fei, Y. W. (2008). Melting behavior of (Mg, Fe)O solid solutions at high pressure. *Geophysical Research Letters*, *35*(13), L13302. https://doi.org/10.1029/2008gl034585